Designing Folding Rings using Polynomial Continuation

Andrew D. Viquerat
Research Associate
Department of Engineering
University of Cambridge

Simon D. Guest*
Reader in Structural Mechanics
Department of Engineering
University of Cambridge
Trumpington Street, Cambridge CB2 1PZ, UK
Email: sdg@eng.cam.ac.uk

Two types of foldable rings are designed using polynomial continuation. The first type of ring, when deployed, forms regular polygons with an even number of sides and is designed by specifying a sequence of orientations which each bar must attain at various stages throughout deployment. A design criterion is that these foldable rings must fold with all bars parallel in the stowed position. At first, all three Euler angles are used to specify bar orientations, but elimination is also used to reduce the number of specified Euler angles to two, allowing greater freedom in the design process. The second type of ring, when deployed, forms doubly plane-symmetric (irregular) polygons. The doubly-symmetric rings are designed using polynomial continuation, but in this example a series of bar end locations (in the stowed position) is used as the design criterion with focus restricted to those rings possessing eight bars.

1 Introduction

Many problems in linkage design can be expressed in polynomial form, with design variables such as lengths, thicknesses and internal angles making up the monomials of the equations. Individual equations can take the form of closure/compatibility equations which define the particular conformation of the linkage, or constraint equations which define particular features the linkage should possess. The power of this approach to linkage design (establishing a set of general closure/constraint equations and directly solving the resulting system of equations for the design variables contained within) lies in its ability to provide not just one, but all of the combinations of design variables which satisfy the problem description. A famous example of the direct solution of systems of polynomial equations to reveal a number of feasible sets of design variables is planar 4-bar point path synthesis, initially achieved using five precision points [1,2], and then a full set of nine points [3]. The authors of each of these articles made use of homotopy continuation methods, but such methods are by no means the only tools available for the solution of systems of kinematic equations. Often, given a sufficiently high quality estimate of the required design variables, a simple application of Newton's method, or a numerical optimisation [4, 5] will lead to a single satisfactory result. Several non-gradient based optimisation methods have also been tried [6, 7].

Where it is possible to manipulate the system of closure/constraint equations representing a linkage design problem into polynomial form, a number of solution techniques is available, each guaranteed to locate all possible solutions. This collection of methods includes Gröbner Bases, Galois Theory [8], and the reduction of entire systems via substitution/elimination to a single univariate *companion matrix* which can then be solved as an eigenvalue problem [9, 10]. Methods of *resultants* have been very popular in the study of kinematics [9, 11–13], and are essentially formalised strategies for performing elimination. While especially efficient for small systems, resultant methods are difficult to generalise for larger systems. A branch of numerical continuation called polynomial continuation has been successfully applied to many problems in kinematics [14–18]. Polynomial continuation is a particularly appealing tool for solving larger systems of equations because it is highly generalisable (new systems can be adapted for solution with a minimum of effort), and also because advances in *polyhedral homotopy* methods [19–22] have dramatically reduced the number of solution paths to be traced. In the following sections, polyno-

*Corresponding author

mial continuation will be used as a tool to design members of a family of (generally underconstrained) foldable rings [23]. The continuation software was written in MATLAB [24]. The polyhedral homotopy algorithm is based largely on work published by Li [19], while the path following algorithm was written specifically for this application

2 Regular-Polygonal Foldable Rings

The type of linkage considered in this section is a cyclic and equilateral ring (that is, it displays rotational symmetry about a line passing through the centre of the ring), generally referred to as a regular polygon. Its purpose is most likely to be the provision of a frame upon which to stretch a membrane such as a flexible solar array or a radar. It could also be used to support a reflecting antenna [25] in which circumstance it might be referred to as a *hoop-column* antenna. The inspiration for the foldable ring examined in this section comes from a deployable *spoked wheel* designed by the Astro Research Corporation for NASA, first described in a conference paper [26], and later in a report [27]. The majority of the report is concerned with a 'two-hinge' design for the ring/wheel, in which adjacent bars are connected to one another by an intermediate hub block with one hinge at each end (possibly connected internally by a form of gearing). A more interesting design challenge comes in the form of a 'single-hinge' ring, in which each bar is connected to its neighbour by a single hinge. An example of a 10-bar version of such a single hinge ring is shown in Figure 1. As can be seen, the ring forms a regular polygon in its deployed configuration, and can be folded such that each of its bars is parallel to the others in the stowed configuration.

In planar 4-bar point path synthesis, up to nine precision points can be specified (in terms of their X and Y locations). Here, to design the regular-polygonal foldable ring, a set of angular 'precision points' is used. These points specify, not any particular locations in physical space, but rather bar orientations in terms of Euler angles. Note that the rotational symmetry of the ring allows the entire ring to be designed in terms of any one of its bars. Any bar of the ring can be reflected $n-1$ times (where n is the number of bars) to generate the rest of the ring. The prescription of angular orientations or bar inclinations to the global axis allows a designer to select the exact shape of the ring at a limited number of poses during deployment. In this way, a designer can attempt to steer the linkage along a certain path during its deployment. It is possible that a number of different ring designs could satisfy the constraints set by the designer; a situation which manifests itself in the appearance of multiple solutions to a system of closure/constraint equations. In general, it cannot be known *a priori* how many, if any, solutions exist to a given problem. Henceforth, the particular bar which has been chosen to represent the entire ring will be referred to as the *design* bar.

The number of bars (n) must be even. While 4-bar and 6-bar variants of the single-hinge foldable ring are overconstrained mechanisms (Bennett and Bricard linkages, respectively), the focus here will be those rings with $n \geq 8$. Since

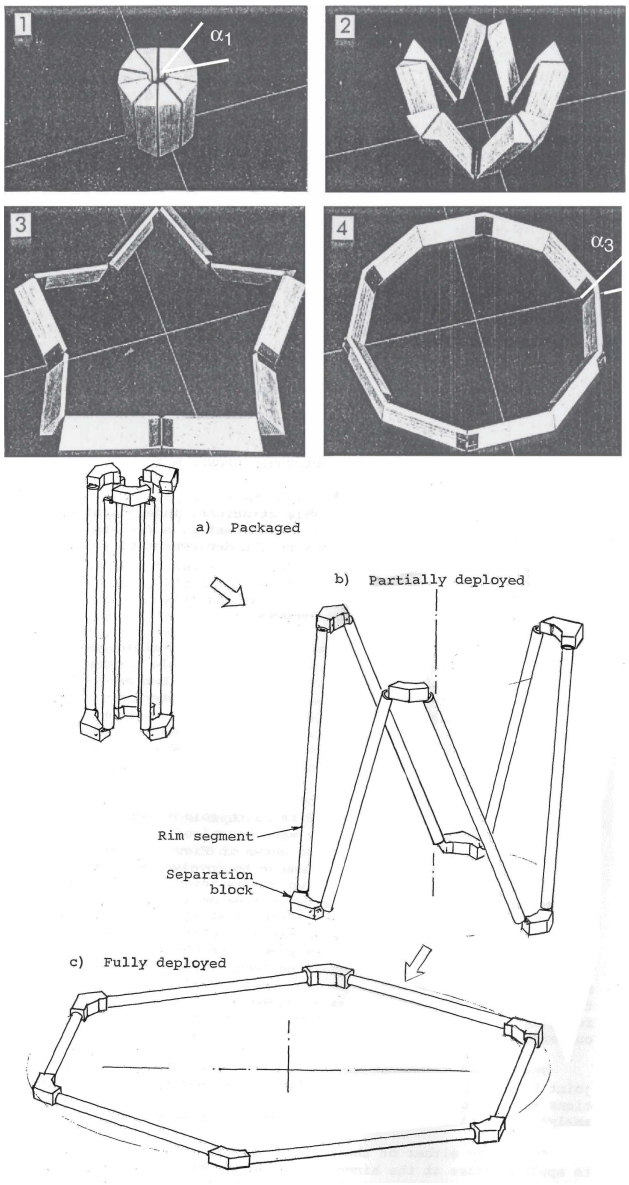

Fig. 1. Top: the deployment of a 10-bar single-hinge ring, the multiple degrees of freedom are not apparent here as the deployment has been carefully controlled, and the linkage supported by the table underneath. Bottom: the deployment of the two-hinge design. (From [27])

any spatial ring with $n \geq 7$ is certain to have at least one degree of freedom, it is likely that a number of cables or *spokes* would be required to constrain the deployment of the ring to a desirable path. The exact nature of this constraint is neglected henceforth (as it is not the main concern of this paper), and is simply assumed to exist.

A top view of the single-hinge regular-polygonal deployable ring is given in Figure 2. The highlighted design bar also has its hinges shown as $\mathbf{h}_l$ on the left and $\mathbf{h}_r$ on the right, where the subscripts l and r denote 'left' and 'right' respectively. It is necessary that the hinge vectors of this bar (and hence those of all the other bars) remain in the planes shown in Figures 2 and 3 during deployment. An isomet-

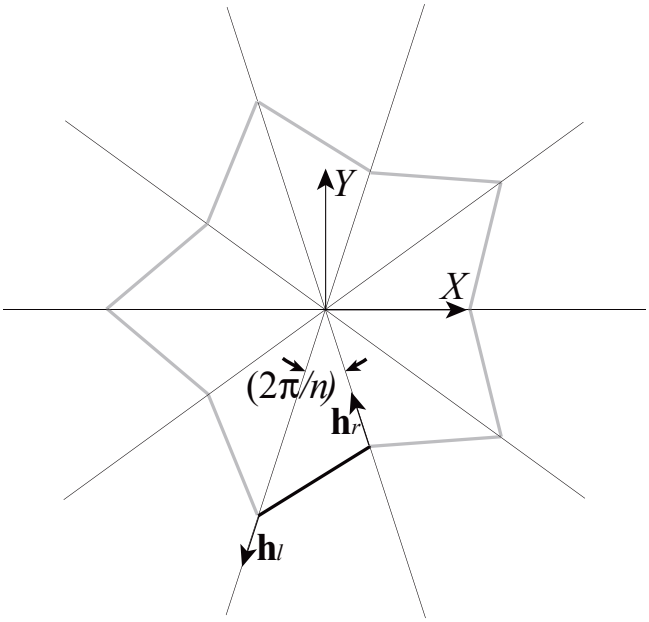

Fig. 2. Top view of regular-polygonal foldable ring (in mid-deployment) with $n = 10$. Global coordinates are indicated.

ric view of the design bar is shown in Figure 3. The hinges

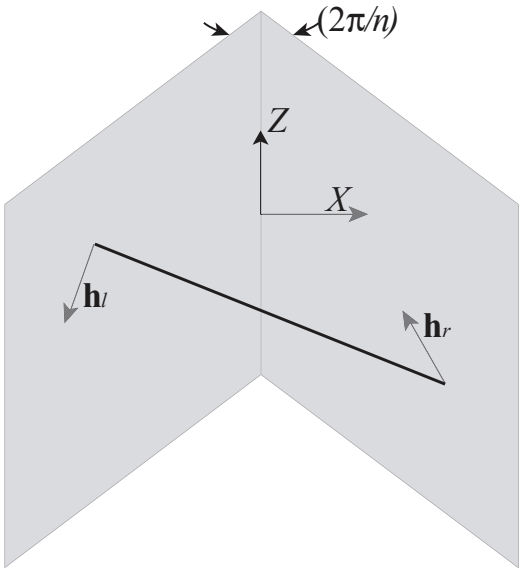

Fig. 3. Isometric view of individual bar in regular-polygonal ring with global coordinates indicated. Two of the planes of reflection are shown. The bar hinge vectors must remain in these planes at all times.

are fixed to the end of each bar. An obvious question arises: is it always possible to find a bar orientation such that the hinges at the ends of the bar lie exactly in each of the two planes shown in Figure 3, and if this is possible, how many different orientations which achieve this are there? It is not immediately clear that there are not an infinite number of orientations. Using polynomial continuation, it can be guaranteed that every one of the possible solutions will be found (including positive dimensional sets which indicate the presence of a continuum of solutions), so they can be enumerated with confidence.

The next stage is to determine an appropriate set of design variables. In this analysis, bar lengths are not considered as variables: the lengths all being made equal to one another, and set to unity without loss of generality. Bar thickness, while being an important consideration for the self-interference of real linkages, is assumed to be infinitesimally small in this analysis. Consider instead the hinges attached to each end of the design bar. To allow for maximum generality, they may have any orientation with respect to the local coordinates of the bar. Figure 4 shows how the hinge vectors are defined in local coordinates x, y, z for the bar. Each

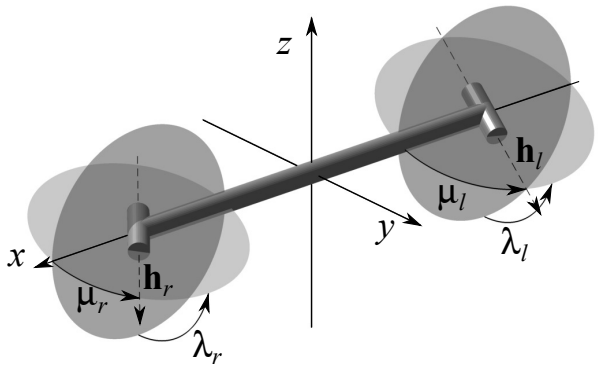

Fig. 4. Regular-polygonal ring bar shown in local coordinates with hinge definitions. Note that the bar has been rotated to show the angle definitions more clearly.

hinge is assigned a 'longitude' λ, and a 'lattitude' μ. Using l and r again to denote the left and right hand ends of the bar; the four design variables are $\{\lambda_l, \mu_l, \lambda_r, \mu_r\}$. The left and right hinges can thus be constructed as unit vectors (in local coordinates attached to the bar):

$$\mathbf{h}_l = \begin{bmatrix} \cos(\mu_l) \\ \sin(\mu_l)\sin(\lambda_l) \\ -\sin(\mu_l)\cos(\lambda_l) \end{bmatrix} \quad \mathbf{h}_r = \begin{bmatrix} \cos(\mu_r) \\ \sin(\mu_r)\sin(\lambda_r) \\ -\sin(\mu_r)\cos(\lambda_r) \end{bmatrix} \tag{1}$$

In order to ensure (mathematically) that the design bar does not venture outside its two partitioning planes (see Figure 3), and that the hinge vectors attached to each end of the design bar lie within each of these planes, it is necessary to introduce two *compatibility* equations. The term 'compatibility' is used because the equations' purpose is to enforce certain constraints at the planes of symmetry, which then ensures that each link is compatible with the next (across the plane of symmetry).

Define a rotation matrix R, which is a function of ϕ (a roll), θ (a pitch), and ψ (a yaw). Specifically:

$$R = R_z(\psi)R_y(\theta)R_x(\phi)$$

where R_x, R_y and R_z perform rotations about the X, Y and Z axes respectively. If the design bar undergoes a rotation defined by R, then so do the hinge vectors at each of its ends. Now assume that the two planes shown in Figure 3 have normal vectors $\mathbf{n}_l$ on the left and $\mathbf{n}_r$ on the right. It is now possible to write the two governing equations for the motion of the bar (based on the fact that each hinge must remain in its respective plane) as:

$$\begin{aligned} \langle R\mathbf{h}_l \ , \ \mathbf{n}_l \rangle &= 0 \\ \langle R\mathbf{h}_r \ , \ \mathbf{n}_r \rangle &= 0 \end{aligned} \tag{2}$$

Together, these equations form the compatibility equations for the ring. As depicted, the plane normals will have the form:

$$\mathbf{n}_l = \begin{bmatrix} \cos(\frac{\pi}{n}) \\ -\sin(\frac{\pi}{n}) \\ 0 \end{bmatrix} \quad \mathbf{n}_r = \begin{bmatrix} \cos(\frac{\pi}{n}) \\ \sin(\frac{\pi}{n}) \\ 0 \end{bmatrix}$$

in global coordinates. The two relationships in Equation 2 are written in terms of the input parameters ϕ, θ and ψ. These three angles allow a designer to completely (although not uniquely) specify the orientation of the design bar, and hence, the exact shape of the foldable ring. While it is not possible to specify the exact shape of a foldable ring at all points during its deployment, by carefully selecting the hinge orientations ($\{\lambda_l, \mu_l, \lambda_r, \mu_r\}$), a designer can create a foldable ring which passes through a set of desired design bar orientations as it deploys.

The remaining question is: how does a designer select λ_l, μ_l, λ_r and μ_r? The compatibility equations (2) are written in terms of ϕ, θ and ψ, as well as the four design variables λ_l, μ_l, λ_r and μ_r. There are two fundamental compatibility equations, three input (orientation) angles and four design variables. There are a number of approaches which may be taken to using the compatibility equations. The main guiding principle is that four independent equations must be formed in order to solve for all four of the design variables. Three different methods will be explored:

1. use the two compatibility equations in their current form, and use two sets of input angles to form two pairs of the compatibility equations, resulting in the required four equations;
2. combine the two compatibility equations into one by eliminating the ψ input angle. This allows for four sets of the remaining inputs $\{\theta, \phi\}$ to be used to generate the required four versions of the reduced single compatibility equation;
3. combine the two compatibility equations into one by eliminating the ϕ input angle. A mixture of $\{\theta, \phi\}$ and $\{\theta, \psi\}$ type reduced compatibility equations is used to design the ring.

2.1 Using the Original Form of the Compatibility Equations

It is possible to choose two sets of orientation (Euler) angles $\{\phi_1, \theta_1, \psi_1\}$ and $\{\phi_2, \theta_2, \psi_2\}$, and then use polynomial continuation to arrive at a set of design variables which describe a bar/ring system which will pass through the prescribed orientations at some point during the ring's deployment. In their current form, the two equations in Equation 2 are decoupled, but will solved simultaneously in this first section to illustrate the use of the continuation method. To ensure pure polynomial form, the sines (S_x) and cosines (C_x) of the design variable angles are used instead of the angles themselves. This doubles the number of unknowns, and requires the addition of equations of the form $C_x^2 + S_x^2 - 1 = 0$. The full set of equations is given below.

$$F = \left\{ \begin{array}{l} \langle R(\phi_1, \theta_1, \psi_1) \dots \\ \quad \mathbf{h}_l(C_{\lambda_l}, S_{\lambda_l}, C_{\mu_l}, S_{\mu_l}, C_{\lambda_r}, S_{\lambda_r}, C_{\mu_r}, S_{\mu_r}) \ , \ \mathbf{n}_l(n) \rangle \\ \langle R(\phi_2, \theta_2, \psi_2) \dots \\ \quad \mathbf{h}_l(C_{\lambda_l}, S_{\lambda_l}, C_{\mu_l}, S_{\mu_l}, C_{\lambda_r}, S_{\lambda_r}, C_{\mu_r}, S_{\mu_r}) \ , \ \mathbf{n}_l(n) \rangle \\ \langle R(\phi_1, \theta_1, \psi_1) \dots \\ \quad \mathbf{h}_r(C_{\lambda_l}, S_{\lambda_l}, C_{\mu_l}, S_{\mu_l}, C_{\lambda_r}, S_{\lambda_r}, C_{\mu_r}, S_{\mu_r}) \ , \ \mathbf{n}_r(n) \rangle \\ \langle R(\phi_2, \theta_2, \psi_2) \dots \\ \quad \mathbf{h}_r(C_{\lambda_l}, S_{\lambda_l}, C_{\mu_l}, S_{\mu_l}, C_{\lambda_r}, S_{\lambda_r}, C_{\mu_r}, S_{\mu_r}) \ , \ \mathbf{n}_r(n) \rangle \\ C_{\lambda_l}^2 + S_{\lambda_l}^2 - 1 \\ C_{\mu_l}^2 + S_{\mu_l}^2 - 1 \\ C_{\lambda_r}^2 + S_{\lambda_r}^2 - 1 \\ C_{\mu_r}^2 + S_{\mu_r}^2 - 1 \end{array} \right\} = \mathbf{0}$$

This system has a total degree of $2^8 = 256$ in the eight unknowns. However, it has a mixed volume of only 16 [28], indicating that the vast majority of the solutions are at infinity.

There are two critical phases to the deployment; fully deployed and fully stowed. Since it is possible to specify two sets of input angles only when using the original form of the compatibility equations, it makes some sense to use these deployment limit points as the design goals. When deployed, the design bar has a pitch (θ) of 0°, and a yaw (ψ) of 0°. The roll (ϕ) is irrelevant. When the bar is stowed, it has a pitch of 90°, and both roll and yaw are irrelevant. As an example, choose the following set of angles (in radians):

$$\begin{bmatrix} \phi_1 \\ \theta_1 \\ \psi_1 \end{bmatrix} = \begin{bmatrix} 0 \\ 0 \\ 0 \end{bmatrix}; \quad \begin{bmatrix} \phi_2 \\ \theta_2 \\ \psi_2 \end{bmatrix} = \begin{bmatrix} \frac{\pi}{2} \\ \frac{\pi}{2} \\ 0 \end{bmatrix} \tag{3}$$

This set gives sixteen real solutions, which all reduce to the same hinge vectors. One solution is:

$$\begin{bmatrix} \lambda_l \\ \mu_l \\ \lambda_r \\ \mu_r \end{bmatrix} = \begin{bmatrix} -18^\circ \\ -84.3^\circ \\ -162^\circ \\ -95.7^\circ \end{bmatrix} \Rightarrow \mathbf{h}_l = \begin{bmatrix} 0.0999 \\ 0.3075 \\ 0.9463 \end{bmatrix} \ , \ \mathbf{h}_r = \begin{bmatrix} -0.0999 \\ 0.3075 \\ -0.9463 \end{bmatrix}$$

This particular solution is identical to that derived using the methods in [29], in which it is assumed that each bar has an (isosceles) triangular cross-section. The symmetry of the solution is obvious. Since this is the only solution to appear in the continuation process, it can be said that the isosceles triangle based design is the only one which satisfies these particular deployed and stowed configuration requirements. The orientation of the design bar during closure is shown in Figure 5, while a sequence of the ring moving from the deployed to stowed configuration is given in Figure 6. It is, of course, possible to choose other sets of input angles, but the set described above illustrates how continuation can

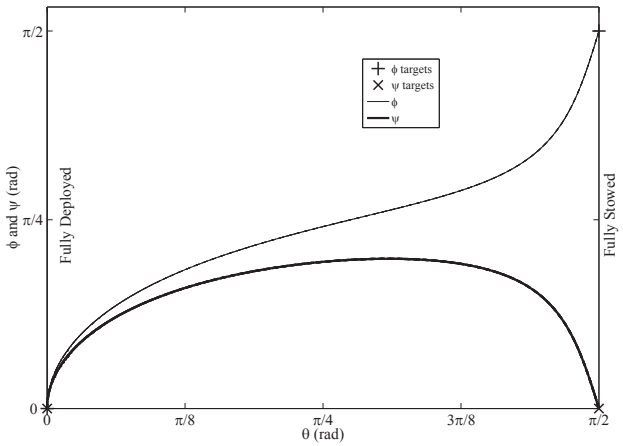

Fig. 5. Example of a ring design using the original compatibility equations ($n = 10$), and the angle targets given in Equation 3.

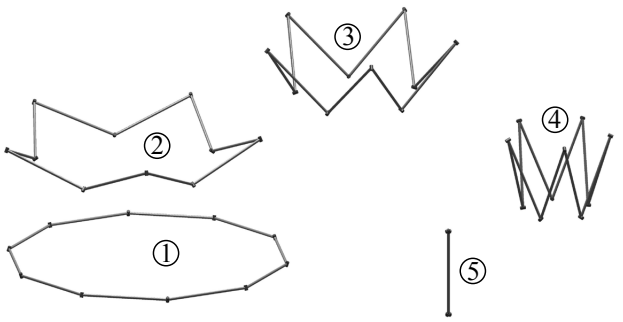

Fig. 6. Example of a fully feasible ring moving from deployed to stowed positions (clockwise from bottom left). It is based on the targets of Equation 3, and its angular progression is shown in Figure 5.

be used to design a ring which could be feasibly constructed and operated and have real practical applications.

Another way to solve the simple case presented in this section is to assume that the fully deployed pose must always be one of the targets. From this deployed pose ($\phi = \theta = \psi = 0$), the hinge unit vectors can be defined in terms of a single rotation from vertical in their respective planes (this method is employed in Section 3). The vectors of Equation 1 can be rewritten as:

$$\mathbf{h}_l = \begin{bmatrix} -\sin(\frac{\pi}{n})\sin(\alpha_l) \\ -\cos(\frac{\pi}{n})\sin(\alpha_l) \\ \cos(\alpha_l) \end{bmatrix} \quad \mathbf{h}_r = \begin{bmatrix} \sin(\frac{\pi}{n})\sin(\alpha_r) \\ -\cos(\frac{\pi}{n})\sin(\alpha_r) \\ \cos(\alpha_r) \end{bmatrix}$$

where α_l and α_r are the rotations of the hinge vectors in the left and right planes. Using the second (stowed) set of target angles from Equation 3, Equation 2 becomes:

$$\begin{aligned} \sin(\alpha_l)\cos^2\left(\frac{\pi}{n}\right) + \cos(\alpha_l)\sin\left(\frac{\pi}{n}\right) &= 0 \\ \cos(\alpha_r)\sin\left(\frac{\pi}{n}\right) - \sin(\alpha_r)\cos^2\left(\frac{\pi}{n}\right) &= 0 \end{aligned}$$

which can be solved separately for the angles α_l and α_r. This implicitly includes the deployed pose in the solution. For generality, no initial pose will be included in the hinge unit vector definitions, and the four design variables of Equation 1 will be retained.

2.2 Using $\{\phi\ ,\ \theta\}$ to Specify Bar Orientation

Sometimes, it is beneficial to reduce the description of the motion of a deployable structure to a single compatibility equation, as this reduces the amount of information which must be specified *a priori* in a design using continuation. If the two compatibility equations in Equation 2 are combined, only two of the three input angles need be specified to define a target point, leaving the third free. To combine the two compatibility equations, one of the three variables; ϕ, θ or ψ must be eliminated. It is interesting to observe what happens when the dependence on ψ is removed.

The equations in 2 can be written as:

$$\begin{bmatrix} m_{l_1} & m_{l_2} \\ m_{r_1} & m_{r_2} \end{bmatrix} \begin{bmatrix} C_\psi \\ S_\psi \end{bmatrix} = \begin{bmatrix} 0 \\ 0 \end{bmatrix}$$

where:

$$\begin{bmatrix} m_{l_1} & m_{l_2} \\ m_{r_1} & m_{r_2} \end{bmatrix} = M(\phi, \theta, \lambda_l, \mu_l, \lambda_r, \mu_r)$$

For this system to have a solution, then

$$\tilde{f} \equiv \det(M) = m_{l_1} m_{r_2} - m_{l_2} m_{r_1} = 0 \tag{4}$$

(this particular elimination technique was also used in [27] as part of a different compatibility equation formulation). Equation 4 is a single compatibility equation for the system, and is written completely in terms of the angular inputs ϕ and θ, as well as the design variables $\{\lambda_l, \mu_l, \lambda_r, \mu_r\}$. The equation has 9 terms. This equation can be used to define a necessary relationship between ϕ and θ at a point in the bar's motion, without specifying anything about the third angular input, ψ.

Once again, eight equations form the continuation target set. This time, four sets of pairs of input angles can be selected: $\{\phi_i, \theta_i\}\ \ i = 1, \ldots, 4$. These sets form the target system as:

$$F = \left\{ \begin{array}{l} \tilde{f}\left(\{\phi_1, \theta_1\}, \{C_{\lambda_l}, S_{\lambda_l}, C_{\mu_l}, S_{\mu_l}, C_{\lambda_r}, S_{\lambda_r}, C_{\mu_r}, S_{\mu_r}\}\right) \\ \tilde{f}\left(\{\phi_2, \theta_2\}, \{C_{\lambda_l}, S_{\lambda_l}, C_{\mu_l}, S_{\mu_l}, C_{\lambda_r}, S_{\lambda_r}, C_{\mu_r}, S_{\mu_r}\}\right) \\ \tilde{f}\left(\{\phi_3, \theta_3\}, \{C_{\lambda_l}, S_{\lambda_l}, C_{\mu_l}, S_{\mu_l}, C_{\lambda_r}, S_{\lambda_r}, C_{\mu_r}, S_{\mu_r}\}\right) \\ \tilde{f}\left(\{\phi_4, \theta_4\}, \{C_{\lambda_l}, S_{\lambda_l}, C_{\mu_l}, S_{\mu_l}, C_{\lambda_r}, S_{\lambda_r}, C_{\mu_r}, S_{\mu_r}\}\right) \\ C_{\lambda_l}^2 + S_{\lambda_l}^2 - 1 \\ C_{\mu_l}^2 + S_{\mu_l}^2 - 1 \\ C_{\lambda_r}^2 + S_{\lambda_r}^2 - 1 \\ C_{\mu_r}^2 + S_{\mu_r}^2 - 1 \end{array} \right\} = \mathbf{0}$$

This system has a total degree of $4^4.2^4 = 4096$, but a mixed volume of only 96. Typically, all 96 solutions of the target system are non-singular and geometrically isolated.

As an example, consider the target angles (again in radians):

$$\begin{bmatrix}\phi_1\\ \theta_1\end{bmatrix} = \begin{bmatrix}0.05\\ 0.1\end{bmatrix}; \quad \begin{bmatrix}\phi_2\\ \theta_2\end{bmatrix} = \begin{bmatrix}0.1\\ 0.3\end{bmatrix}; \quad \begin{bmatrix}\phi_3\\ \theta_3\end{bmatrix} = \begin{bmatrix}0.3\\ 0.7\end{bmatrix}; \quad \begin{bmatrix}\phi_4\\ \theta_4\end{bmatrix} = \begin{bmatrix}0.5\\ 1.2\end{bmatrix} \tag{5}$$

which produces the result shown in Figure 7. Although there are two separate ϕ paths which hit all of the input angle targets, neither design could be said to be feasible, primarily because neither progresses all the way to $\theta = \pi/2$ (the fully stowed configuration).

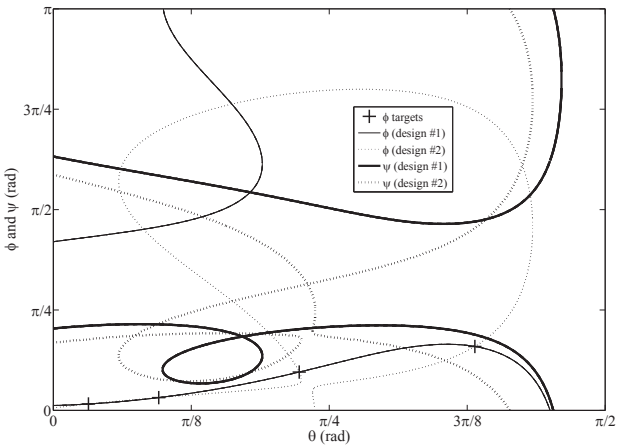

Fig. 7. Example of system designed with four $\{\phi, \theta\}$ specifications ($n = 10$), and the angle targets given in Equation 5.

Next, alter the target angles slightly to include one target pair at $\theta = \pi/2$:

$$\begin{bmatrix}\phi_1\\ \theta_1\end{bmatrix} = \begin{bmatrix}0.05\\ 0.1\end{bmatrix}; \quad \begin{bmatrix}\phi_2\\ \theta_2\end{bmatrix} = \begin{bmatrix}0.1\\ 0.3\end{bmatrix}; \quad \begin{bmatrix}\phi_3\\ \theta_3\end{bmatrix} = \begin{bmatrix}0.3\\ 0.7\end{bmatrix}; \quad \begin{bmatrix}\phi_4\\ \theta_4\end{bmatrix} = \begin{bmatrix}0.5\\ \frac{\pi}{2}\end{bmatrix} \tag{6}$$

with the result shown in Figure 8. In this case there are actually four separate ϕ paths which hit the first three targets, but none which hit the fourth at $\theta = \pi/2$. This illustrates an interesting feature. It happens that:

$$\left.\frac{\partial \tilde{f}}{\partial \phi}\right|_{\theta=\frac{\pi}{2}} = 0$$

This means that the specification of any value of ϕ is irrelevant when $\theta = \pi/2$ as the equation exhibits no sensitivity to ϕ. Any value of ϕ_4 in the example above will produce the same results as those shown in Figure 8. The advantage of using Equation set 6 as opposed to Equation set 5 is that the former ensures that a proper stowed shape ($\theta = \pi/2$) is reached, even though ϕ is unspecifiable at that point.

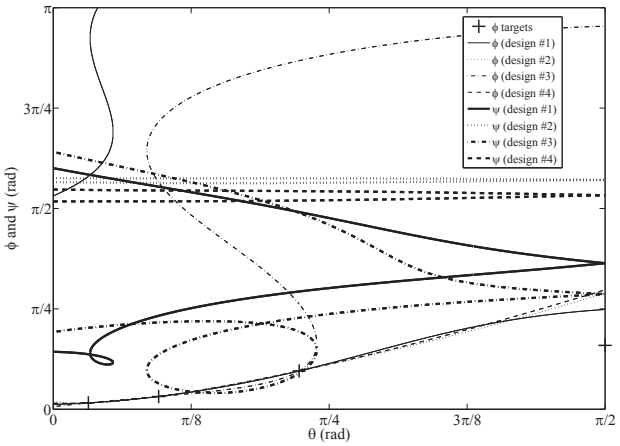

Fig. 8. Second example of system designed with four $\{\phi, \theta\}$ specifications ($n = 10$), and the angle targets given in Equation 6.

2.3 Using $\{\theta\ ,\ \psi\}$ to Specify Bar Orientation

To ensure a proper deployed ring shape, the variable ψ must be specifiable. The two original compatibility equations can be combined by way of the elimination of the variable ϕ. The power of this reduction is that it allows the yaw angle to be specified at a particular pitch angle. This is particularly useful for ensuring that the ring forms a regular polygon when fully deployed by enforcing a zero yaw angle at zero pitch (fully deployed). The elimination of the angle ϕ from the governing Equations 2 is more involved than the elimination of ψ, but demonstrates the way in which new unknowns can be introduced to pose a compatibility equation in pure polynomial form.

Start with the left hinge constraint, and condense its notation as follows:

$$\langle R\mathbf{h}_l\ ,\ \mathbf{n}_l\rangle = w_{l_0} + w_{l_1}C_\phi + w_{l_2}S_\phi = 0$$

The w_{l_i} terms represent combinations of trigonometric functions of the input angles θ and ψ, and the design variables. The explicit expressions are omitted for brevity. Next, make the substitution $C_\phi = m$ and $S_\phi = \sqrt{1-m^2}$, which after rearranging gives:

$$(w_{l_1}^2 + w_{l_2}^2)m^2 + 2w_{l_0}w_{l_1}m + w_{l_0}^2 - w_{l_2}^2 = \zeta_2 m^2 + \zeta_1 m + \zeta_0 = 0$$

where

$$\zeta_2 = w_{l_1}^2 + w_{l_2}^2$$
$$\zeta_1 = 2w_{l_0}w_{l_1}$$
$$\zeta_0 = w_{l_0}^2 - w_{l_2}^2$$

Similar treatment of the equation for the right hinge leads to a second quadratic in m of the form:

$$\xi_2 m^2 + \xi_1 m + \xi_0 = 0$$

Solving each quadratic for m and equating the results gives:

$$\frac{-\zeta_1 \pm \sqrt{\zeta_1^2 - 4\zeta_0\zeta_2}}{2\zeta_2} = \frac{-\xi_1 \pm \sqrt{\xi_1^2 - 4\xi_0\xi_2}}{2\xi_2} \tag{7}$$

At this stage, introduce the new unknowns:

$$\Gamma^2 = \zeta_1^2 - 4\zeta_0\zeta_2$$
$$\Omega^2 = \xi_1^2 - 4\xi_0\xi_2$$

If these new variables are substituted into Equation 7, then the compatibility equation system can be written as:

$$\check{f} \equiv \xi_2 (\Gamma - \zeta_1) - \zeta_2 (\Omega - \xi_1) = 0$$

and

$$\Gamma^2 - \zeta_1^2 + 4\zeta_0\zeta_2 = 0$$
$$\Omega^2 - \xi_1^2 + 4\xi_0\xi_2 = 0$$

which are all pure polynomials written completely in terms of the angular inputs ψ and θ, as well as the design variables $\{\lambda_l, \mu_l, \lambda_r, \mu_r\}$.

Clearly it is going to be more computationally expensive to specify design precision points in terms of $\{\theta, \psi\}$ pairs than $\{\phi, \theta\}$ pairs, as the number of design variables, and hence equations, will increase by two for each pair. As a compromise, a system of target equations which is a combination of the $\{\phi, \theta\}$ and $\{\theta, \psi\}$ based compatibility equations will be used:

$$F = \begin{Bmatrix} \tilde{f}\left(\{\phi_1, \theta_1\}, \{C_{\lambda_l}, S_{\lambda_l}, C_{\mu_l}, S_{\mu_l}, C_{\lambda_r}, S_{\lambda_r}, C_{\mu_r}, S_{\mu_r}\}\right) \\ \tilde{f}\left(\{\phi_2, \theta_2\}, \{C_{\lambda_l}, S_{\lambda_l}, C_{\mu_l}, S_{\mu_l}, C_{\lambda_r}, S_{\lambda_r}, C_{\mu_r}, S_{\mu_r}\}\right) \\ \tilde{f}\left(\{\phi_3, \theta_3\}, \{C_{\lambda_l}, S_{\lambda_l}, C_{\mu_l}, S_{\mu_l}, C_{\lambda_r}, S_{\lambda_r}, C_{\mu_r}, S_{\mu_r}\}\right) \\ \check{f}\left(\{\psi_1, \theta_4\}, \{C_{\lambda_l}, S_{\lambda_l}, C_{\mu_l}, S_{\mu_l}, C_{\lambda_r}, S_{\lambda_r}, C_{\mu_r}, S_{\mu_r}\}\right) \\ \Gamma^2 - \zeta_1^2 + 4\zeta_0\zeta_2 \\ \Omega^2 - \xi_1^2 + 4\xi_0\xi_2 \\ C_{\lambda_l}^2 + S_{\lambda_l}^2 - 1 \\ C_{\mu_l}^2 + S_{\mu_l}^2 - 1 \\ C_{\lambda_r}^2 + S_{\lambda_r}^2 - 1 \\ C_{\mu_r}^2 + S_{\mu_r}^2 - 1 \end{Bmatrix} = \mathbf{0}$$

This system has an impressive total degree of $4^3.7.8.8.2^4 = 458752$, but a mixed volume of only 768. Using this system, it is possible to specify what the yaw angle should be at one particular pitch angle, as well as what the roll should be at a further three pitches. This gives a very large degree of control over the motion of the ring.

As an example, consider the target angles:

$$\begin{bmatrix} \psi_1 \\ \theta_1 \end{bmatrix} = \begin{bmatrix} 0 \\ 0 \end{bmatrix}; \quad \begin{bmatrix} \phi_1 \\ \theta_2 \end{bmatrix} = \begin{bmatrix} \frac{\pi}{16} \\ \frac{\pi}{8} \end{bmatrix}; \quad \begin{bmatrix} \phi_2 \\ \theta_3 \end{bmatrix} = \begin{bmatrix} \frac{\pi}{8} \\ \frac{\pi}{4} \end{bmatrix}; \quad \begin{bmatrix} \phi_3 \\ \theta_4 \end{bmatrix} = \begin{bmatrix} \frac{3\pi}{16} \\ \frac{3\pi}{8} \end{bmatrix} \tag{8}$$

This generates the paths shown in Figure 9. One of the two separate designs shown here which hit the various targets, actually gets quite close to full closure at $\theta = \pi/2$ by chance, but just fails to achieve full closure. Notice, however, that the ψ paths pass through $\psi = 0$ at full deployment, which is very likely to be a desirable design criterion for the ring. To actually ensure full closure, one of the target equations needs to specify $\theta = \pi/2$, as in:

$$\begin{bmatrix} \psi_1 \\ \theta_1 \end{bmatrix} = \begin{bmatrix} 0 \\ 0 \end{bmatrix}; \quad \begin{bmatrix} \phi_1 \\ \theta_2 \end{bmatrix} = \begin{bmatrix} 0.25 \\ \frac{\pi}{6} \end{bmatrix}; \quad \begin{bmatrix} \phi_2 \\ \theta_3 \end{bmatrix} = \begin{bmatrix} 0.5 \\ \frac{\pi}{3} \end{bmatrix}; \quad \begin{bmatrix} \phi_3 \\ \theta_4 \end{bmatrix} = \begin{bmatrix} - \\ \frac{\pi}{2} \end{bmatrix} \tag{9}$$

which results in the two separate ring designs shown in Figure 10. While both designs reach a fully stowed position

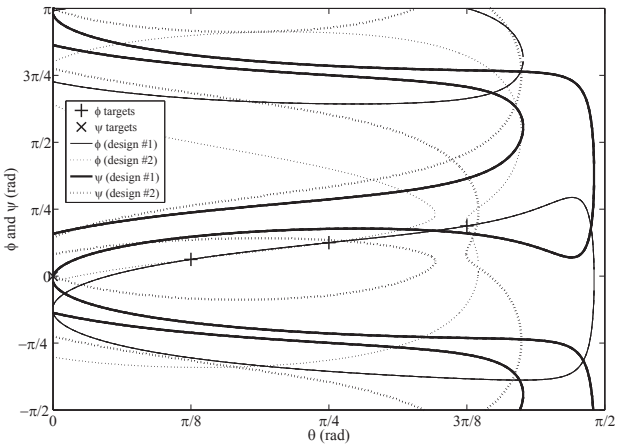

Fig. 9. Example of system designed with three $\{\phi, \theta\}$ specifications and one $\{\theta, \psi\}$ ($n = 10$), and the angle targets given in Equation 8.

with $\theta = \pi/2$, only one of the two designs starts with $\psi = 0$ in the deployed position (labelled as design # 1), so only one completely satisfies the design requirements. This feasible design is represented in a deployment sequence in Figure 11. The feasible ring has the hinge vectors:

$$\begin{bmatrix} \lambda_l \\ \mu_l \\ \lambda_r \\ \mu_r \end{bmatrix} = \begin{bmatrix} 136.78^\circ \\ -96.80^\circ \\ 172.78^\circ \\ -94.64^\circ \end{bmatrix}$$
$$\Rightarrow \mathbf{h}_l = \begin{bmatrix} -0.1184 \\ -0.6800 \\ -0.7236 \end{bmatrix}, \ \mathbf{h}_r = \begin{bmatrix} -0.0809 \\ -0.1253 \\ -0.9888 \end{bmatrix}$$

Once again, the value of ϕ_1 specified is irrelevant since $\tilde{f}$ is

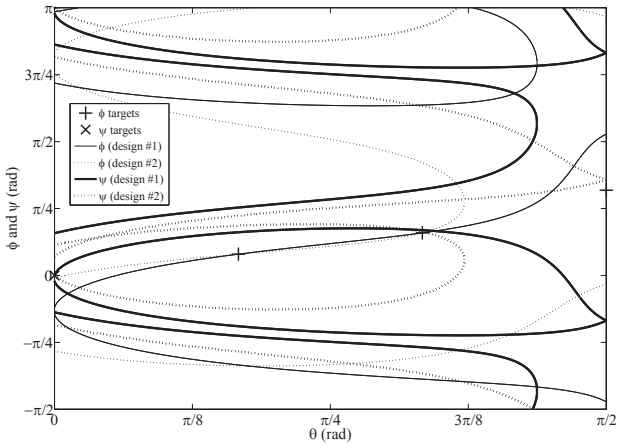

Fig. 10. Second example of system designed with three $\{\phi, \theta\}$ specifications and one $\{\theta, \psi\}$ ($n = 10$), and the angle targets given in Equation 9.

completely insensitive to ϕ when $\theta = \pi/2$. In this case, what has been designed is a completely functional ring which has all bars parallel in its fully stowed state, and forms a regular polygon when deployed.

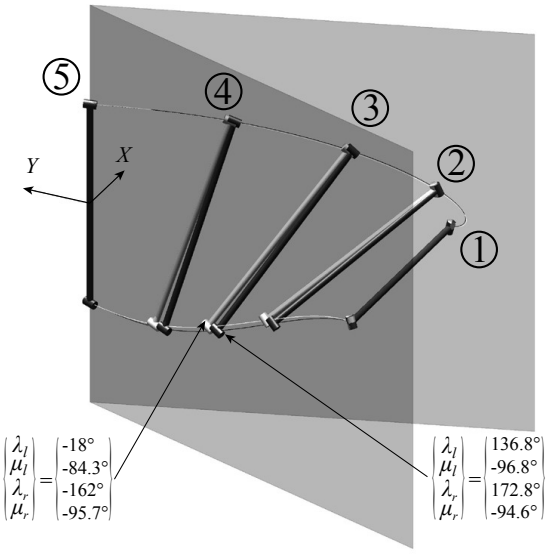

Fig. 11. The deployment sequence of design #1 in Figure 10 (in black, based on target set in Equation 9) is, coincidentally, quite similar to that in Figure 6 (in white). By focussing on the deployment of a single bar it is possible to observe the differences between the two designs. The two λ_l and λ_r angles are quite different, while the deployed states of each design appear quite similar. This is because the roll angles (ϕ) applied to each design bring them into closer alignment. (Note that the five poses shown here do not correspond to the target poses used in the design process)

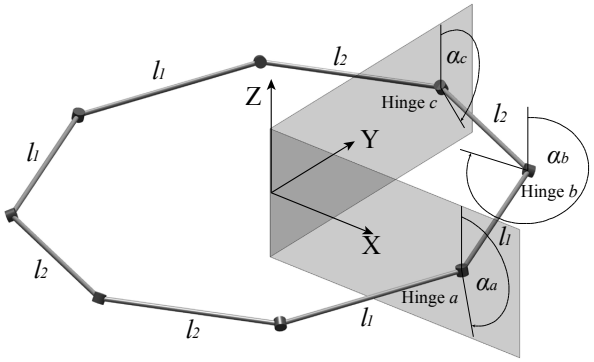

Fig. 12. The doubly symmetric 8-bar foldable loop in the deployed configuration. Hinge inclinations to the vertical are shown. The two perpendicular planes of symmetry are shown bounding the first XY quadrant. Bar lengths l_1 and l_2 are also labelled.

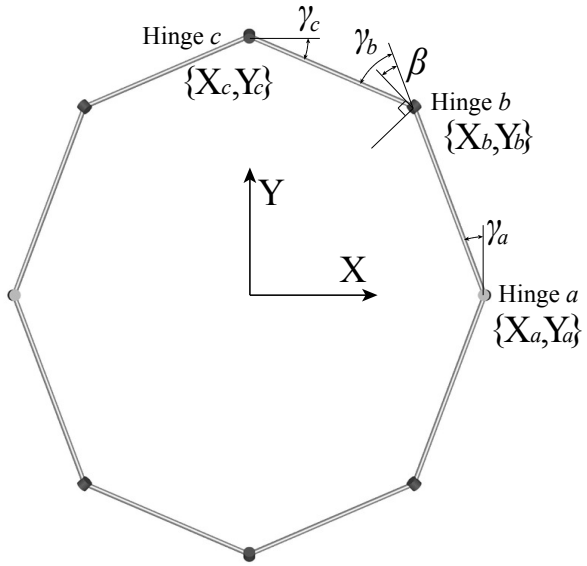

Fig. 13. The doubly symmetric 8-bar foldable loop in the deployed configuration. Hinge XY plane locations are shown.

3 Doubly Symmetric 8-Bar Foldable Rings

The requirement that the foldable ring be a regular polygon (when deployed) is now relaxed. The relaxation greatly increases the variety of rings which might be considered, and allows, for instance, frames supporting almost any shape of membrane. Of interest are frames which are able to fold up into a compact stowed shape (although not necessarily with all bars completely parallel, as in the previous section). To rein in the scope of the problem, two perpendicular planes of symmetry are introduced, with their intersection defining a central axis. The two-fold plane symmetry means that the number of bars will always be a multiple of four. The case of the 8-bar foldable ring is presented here.

The ring's deployed position is used as the basis for its specification. The design parameters for this ring are shown in Figures 12 and 13, the latter being a top view showing the locations of the vertices in XY coordinates (capitalisation denoting global coordinates). Single hinges, each with a single rotational degree of freedom, connect each bar to the next. Hinges a, b and c all lie in the XY plane in the deployed position. The only constraints placed on the positioning of the vertices are that hinge a must lie on the X axis, meaning $Y_a = 0$, and hinge c must lie on the Y axis, meaning $X_c = 0$. This leaves four initial positional parameters for the loop, $\{X_a, X_b, Y_b, Y_c\}$.

To illustrate a further way in which continuation can be used to design foldable rings, the rings in this section will be designed by way of a precise specification of the stowed ring's shape. In other words, all the design effort will go into defining a single position, rather than a sequence of positions as in Section 2. In a further departure from the methods of Section 2, constraints will take the form of distance relations, or exact node positions, rather than bar orientations. The entire loop can be designed by focusing on the first XY plane quadrant (as shown in Figure 13), and reflecting the result in the XZ and YZ planes to generate the rest of the ring. Setting the locations of the vertices (a, b and c) automatically defines the bar lengths l_1 and l_2, as well as the angles γ_a, γ_b and γ_c. The parameters $\alpha_a, \alpha_b, \alpha_c$ and β, and the hinge rotations ϕ_a, ϕ_b and ϕ_c are the design variables which remain to be determined. The hinge rotations are all considered to be zero in the deployed configuration. In the design of a loop which

is capable of folding up into a tight bundle, hinge b must be able to rotate such that bars 1 (length l_1) and 2 (length l_2) are parallel and coincident. It can be shown that for this to occur, it is necessary that $\beta = \gamma_b/2$. The intention is not to produce a stowed shape in which bars 1 and 2 are completely parallel. However, setting β to $\gamma_b/2$ simplifies the process while ensuring that the stowed shape is a relatively compact bundle of bars.

It is useful to define a series of basis vectors for the ring. Let $\{\mathbf{e}_X^{(G)}, \mathbf{e}_Y^{(G)} \mathbf{e}_Z^{(G)}\}$ define the global basis. Next, define two local axes, with their origins at points a and c respectively. These axes are free to rotate, save that their bases must follow:

$$\mathbf{e}_y^{(a)} = \mathbf{e}_Y^{(G)}$$
$$\mathbf{e}_y^{(c)} = -\mathbf{e}_X^{(G)}$$

The vectors $\mathbf{e}_z^{(a)}$ and $\mathbf{e}_z^{(c)}$ define the hinge axes at points a and c. One can construct a similar basis at point b.

A collection of matrix operators can be defined to simplify later expressions.

$$\begin{aligned}
&a) \quad T_{(a)}^{(c)}(\{l_1, l_2, \gamma_a, \gamma_b, \gamma_c\}, \{\phi_a, \phi_b, \phi_c, \alpha_a, \alpha_b, \alpha_c\}) \\
&b) \quad T_{(b)}^{(a)}(\{l_1, \gamma_a, \gamma_b\}, \{\phi_a, \phi_b, \alpha_a, \alpha_b\}) \\
&c) \quad T_{(b)}^{(c)}(\{l_2, \gamma_b, \gamma_c\}, \{\phi_b, \phi_c, \alpha_b, \alpha_c\}) \\
&d) \quad T_{(c)}^{(a)}(\{l_1, l_2, \gamma_a, \gamma_b, \gamma_c\}, \{\phi_a, \phi_b, \phi_c, \alpha_a, \alpha_b, \alpha_c\}) \\
&e) \quad R_{(c)}^{(a)}(\{\gamma_a, \gamma_b, \gamma_c\}, \{\phi_a, \phi_b, \phi_c, \alpha_a, \alpha_b, \alpha_c\})
\end{aligned} \tag{10}$$

where $T_{(a)}^{(c)}$ is a (4×4) coordinate transformation matrix which converts locations expressed in the coordinates attached to a to those attached to c. Based on this, $T_{(a)}^{(c)}\mathbf{0}$ would give the location of the origin of coordinate system a (and hence, hinge a) in the basis attached to c. Similarly for $T_{(b)}^{(a)}$, $T_{(b)}^{(c)}$ and $T_{(c)}^{(a)}$. For example, if $T_y(\alpha_i, d_y)$ performs a rotation of α_i about the y axis, and a translation d_y along it, and $T_z(\gamma_i, d_z)$ acts similarly on the z axis, then $T_{(c)}^{(a)}$ can be expressed as:

$$\begin{aligned}
T_{(c)}^{(a)} = {} & T_z(\phi_a, 0) T_y(-\alpha_a, 0) T_z(\gamma_a, 0) T_y(0, l_1) T_z(\gamma_b/2, 0) \ldots \\
& T_y(\alpha_b, 0) T_z(\phi_b, 0) T_y(-\alpha_b, 0) T_z(\gamma_b/2, 0) T_y(0, l_2) \ldots \\
& T_z(\gamma_c, 0) T_y(\alpha_c, 0) T_z(\phi_c, 0)
\end{aligned} \tag{11}$$

$R_{(c)}^{(a)}$ is a (3×3) rotation matrix which converts orientations expressed in the coordinates attached to c to those attached to a. The defining compatibility equation for the ring can now be expressed as:

$$\bar{f}_e \equiv R_{(c)}^{(a)} \mathbf{e}_y^{(c)} \cdot \mathbf{e}_y^{(a)} = 0 \tag{12}$$

This equation enforces the double plane symmetry shown in Figures 12 and 13. It forces $\mathbf{e}_y^{(c)}$ and $\mathbf{e}_y^{(a)}$ to be perpendicular at all times, which subsequently forces $\mathbf{e}_z^{(c)}$ and $\mathbf{e}_z^{(a)}$ (the hinge vectors) to lie in the planes depicted.

Some thought can now be given to the kind of foldable 8-bar a designer might like to construct. Firstly, it is likely that most applications will require a convex polygonal deployed shape. Next, the relationship between any driven and passive hinges should be as simple as possible to aid deployment. It is also likely that any practical 8-bar loop of this type will not be required to fold into as tightly packed a bundle as possible, i.e. with bars stowed perfectly parallel. Some space will be left in the centre of the stowed linkage to accommodate a central deployment assistance mechanism, or a folded flexible sheet. A top view of a stowed linkage is given in Figure 14, showing the dimensions of the internal space. Lastly, any of the results derived using continuation will have to be checked for faults such as bar collisions, which cannot easily be accounted for in the continuation process.

(a) 8-bar linkage in stowed configuration (side view).

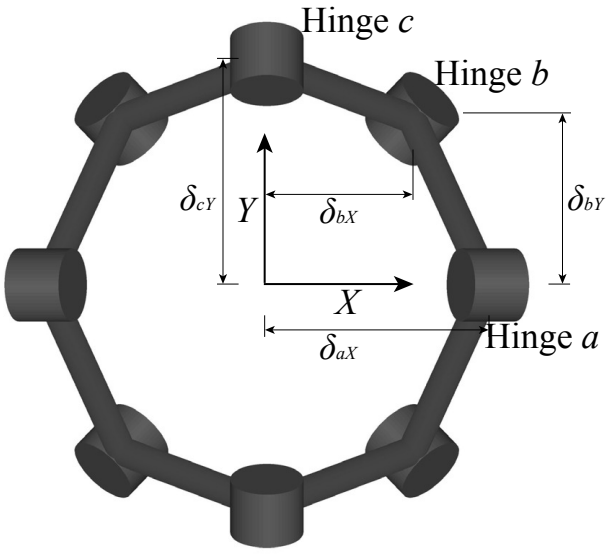

(b) 8-bar linkage in stowed configuration (top view).

Fig. 14. Key dimensions of 8-bar in stowed configuration.

In Section 2, Euler angles were used to specify bar orientations (in global coordinates) as precision points. In a departure from this kind of precision point design method, the doubly symmetric 8-bar foldable ring in this section is designed by way of an exact specification of the linkage's stowed shape. Constraint equations can be written in terms of distances rather than angles (although the design variables themselves will again be angles). By choosing to focus only on the stowed shape, all control over the deployment path is relinquished. Choice of deployment path is relegated to the second more subjective, stage of the continuation design process in which designs may be chosen from amongst the continuation-derived results.

To achieve the stowed configuration shown in Figure 14, it is necessary to introduce three further unknowns in the form of the hinge angles in the stowed position, ϕ_{as}, ϕ_{bs} and ϕ_{cs}. This makes a total of six unknowns; $\{\phi_{as},\phi_{bs},\phi_{cs},\alpha_a,\alpha_b,\alpha_c\}$. If one assumes that the locations of the hinges a, b and c have been set (which directly determines the parameters $\{l_1,l_2,\gamma_a,\gamma_b,\gamma_c\}$), then only these six unknowns remain to be found. Making use of the dimensions shown in Figure 14, it is possible to construct a system of constraint equations which define the stowed shape:

$$\left.\begin{array}{ll}
\bar{f}_a(\{l_1,\gamma_b,\gamma_c\},\dots & \\
\quad \{\phi_{bs},\phi_{cs},\alpha_b,\alpha_c\}) & \equiv T_{(a)}^{(c)}\mathbf{0}\cdot\mathbf{e}_y^{(c)}+\delta_{aX} \\
\bar{f}_b(\{l_1,\gamma_a\},\{\phi_{as},\alpha_a\}) & \equiv T_{(b)}^{(a)}\mathbf{0}\cdot\mathbf{e}_y^{(a)}-\delta_{bY} \\
\bar{f}_c(\{l_2,\gamma_c\},\{\phi_{cs},\alpha_c\}) & \equiv \dfrac{Y_b}{X_b}T_{(b)}^{(c)}\mathbf{0}\cdot\mathbf{e}_y^{(c)}+\delta_{bY} \\
\bar{f}_d(\{l_1,l_2,\gamma_a,\gamma_b\},\dots & \\
\quad \{\phi_{as},\phi_{bs},\alpha_a,\alpha_b\}) & \equiv T_{(c)}^{(a)}\mathbf{0}\cdot\mathbf{e}_y^{(a)}-\delta_{cY}
\end{array}\right\}=\mathbf{0} \quad (13)$$

Note that there are fewer arguments to each of these functions than there are to each corresponding matrix in Equation 10. This is because it is only the origin of each hinge's coordinate system that is of interest in each case. Equation $\bar{f}_a$ is expressed in the coordinates of the local axes attached to hinge c, and sets the distance hinge a should sit away from the origin in the X direction in the stowed configuration. Equation $\bar{f}_b$ is expressed in the coordinates of the local axes attached to hinge a, and sets the distance hinge b should sit away from the X axis when stowed. Equation $\bar{f}_c$ is in local hinge c coordinates, and sets the distance hinge b sits away from the Y axis when stowed. The Y_b/X_b factor included here ensures that the position of hinge b in the deployed and stowed configurations, and the global origin, are collinear. The inclusion of the Y_b/X_b factor also means that the offset δ_{bX} does not need to be specified explicitly. Equation $\bar{f}_d$ is in local hinge a coordinates, and sets the offset of hinge c from the X axis when stowed.

The four constraint and single compatibility equations given above are sufficient to specify a foldable linkage with several desirable characteristics. These five equations, together with the six design variables $\{\phi_{as},\phi_{bs},\phi_{cs},\alpha_a,\alpha_b,\alpha_c\}$, form an under-determined system which could be used to design a family of linkage designs. As an alternative, an additional constraint is introduced which simply has the form:

$$\phi_c=\phi_a$$

which enforces the symmetry and foldability of the linkage. Stipulating that the hinge angles at a and c must be the same at all times may have some practical advantages. If these hinges were, say, driven by motors at the same rate, or if some form of mechanical coupling existed between them, the linkage would behave as though it had a single degree of freedom, and expand to be rigid. The four hinge b's could be left free to rotate. This new equality reduces the number of design variables to five, resulting in a square system of equations.

The form of Equation $\bar{f}_c$, together with the constraint $\phi_c=\phi_a$, has an interesting consequence in terms of the motion of hinge b during deployment. This combination is the equivalent, mathematically, to including a further constraint equation requiring the projection of hinge b onto the XY plane to remain on the same line (formed by the hinge b location when deployed, and the origin) at all times during deployment (hinge b expands radially away from the centre during deployment). This equivalence can be observed by actually constructing such a constraint equation, and noting that its gradient with respect to $\{\phi_{a/c},\phi_b,\alpha_a,\alpha_b,\alpha_c\}$ is always spanned by any four of the five rows of the Jacobian formed by the other five equations.

Explicitly, the full set of target equations for the doubly symmetric 8-bar foldable ring is given by:

$$F=\left\{\begin{array}{l}
\bar{f}_a\left(\{l_1,\gamma_b,\gamma_c\},\{C_{\phi_{bs}},S_{\phi_{bs}},C_{\alpha_b},S_{\alpha_b},C_{\alpha_c},S_{\alpha_c}\}\right) \\
\bar{f}_b\left(\{l_1,\gamma_a\},\{C_{\phi_{as}},S_{\phi_{as}},C_{\alpha_a},S_{\alpha_a}\}\right) \\
\bar{f}_c\left(\{l_2,\gamma_c\},\{C_{\alpha_c},S_{\alpha_c}\}\right) \\
\bar{f}_d\left(\{l_1,l_2,\gamma_a,\gamma_b\},\dots\right. \\
\quad \left.\{C_{\phi_{as}},S_{\phi_{as}},C_{\phi_{bs}},S_{\phi_{bs}},C_{\alpha_a},S_{\alpha_a},C_{\alpha_b},S_{\alpha_b}\}\right) \\
\bar{f}_e\left(\{\gamma_a,\gamma_b,\gamma_c\},\dots\right. \\
\quad \left.\{C_{\phi_{as}},S_{\phi_{as}},C_{\phi_{bs}},S_{\phi_{bs}},C_{\alpha_a},S_{\alpha_a},C_{\alpha_b},S_{\alpha_b},C_{\alpha_c},S_{\alpha_c}\}\right) \\
C_{\phi_{as}}^2+S_{\phi_{as}}^2-1 \\
C_{\phi_{bs}}^2+S_{\phi_{bs}}^2-1 \\
C_{\alpha_a}^2+S_{\alpha_a}^2-1 \\
C_{\alpha_b}^2+S_{\alpha_b}^2-1 \\
C_{\alpha_c}^2+S_{\alpha_c}^2-1
\end{array}\right\}=\mathbf{0}$$

This system of ten equations in ten unknowns has a total degree of 22400, but a mixed volume of only 512. The system was initially given random complex coefficients and solved using polyhedral homotopy techniques. The real-coefficient systems described below were solved by constructing a coefficient homotopy from the initial complex-coefficient system.

3.1 Continuation Results for Arbitrarily Positioned Vertices

To test the design method, some random vertex locations were selected, with the proviso that the deployed linkage be a convex polygon. The initial parameters for this first example are given in Table 1. The particular value of the δ_{bY} offset was chosen in this case because it causes hinge b to be situated a distance of 0.15 units radially from the Z axis (the

Parameter	Value
Hinge a location	$\{1,0\}$
Hinge b location	$\{0.8,0.4\}$
Hinge c location	$\{0,0.8\}$
δ_{aX}	0.15
δ_{bY}	0.06708
δ_{cY}	0.15

Table 1. Initial parameters for 8-bar design example with arbitrarily positioned vertices.

same distance as hinges a and c). This system yielded 32 geometrically isolated solutions. The 32 geometrically isolated solutions were found to reduce to four distinct real designs, with their deployment paths shown in Figure 15. Only one of

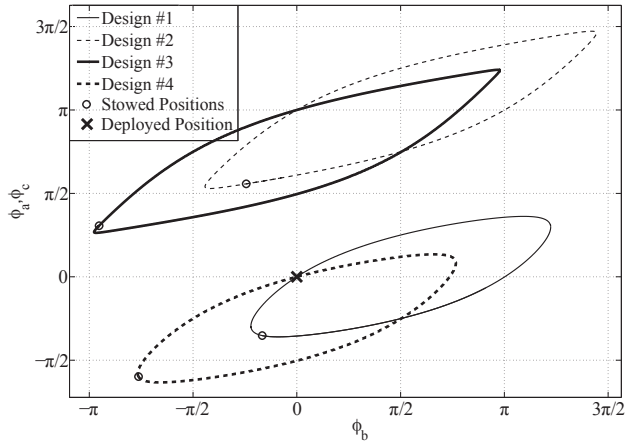

(a) The four distinct solutions

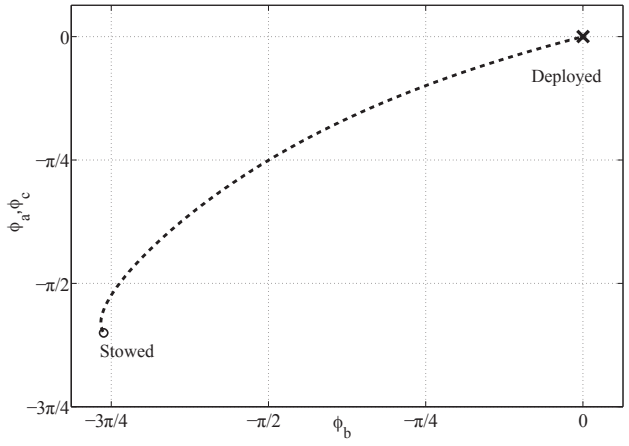

(b) Detail of only feasible solution

Fig. 15. Internal angles for doubly symmetric 8-bar foldable ring with arbitrarily positioned vertices. All simulations were started at the ring stowed positions. Only design # 4 was found to progress satisfactorily from the stowed to deployed configuration.

the finite, real solutions (labelled as design # 4) was found to satisfy the constraints, and to operate in a totally satisfactory manner. That is to say, all hinges open smoothly from stowed to deployed, and all hinges stay within their own quadrant at all times during deployment. As expected, the vertical projection of hinge b onto the XY plane followed the line described by $Y = Y_b/X_b.X$, with only the height above this plane varying. A summary of the details for the single feasible design found is given in Table 2. The deployment is shown in Figure 16.

Parameter	Value (rad)
ϕ_{as},ϕ_{cs}	-1.8797
ϕ_{bs}	-2.3971
α_a	0.1400
α_b	-2.2821
α_c	-0.1400

Table 2. Design variables for 8-bar with arbitrarily positioned vertices, design # 4.

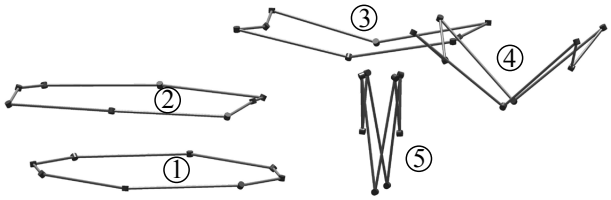

Fig. 16. Folding of 8-bar with arbitrarily positioned vertices, example design # 4; clockwise from bottom left.

3.2 Continuation Results for Rectangular 8-Bars

One particularly interesting subset of the 8-bar foldable loop is the one for which:

$$\gamma_a = 0$$
$$\gamma_b = \pi/2$$
$$\gamma_c = 0$$

This describes a linkage which is rectangular in the deployed configuration. A rectangular linkage can be designed using polynomial continuation in much the same way as a linkage with arbitrarily positioned vertices. The only difference is that the new special values of the γ angles cause $\bar{f}_b$ (Equation 13) to become equivalent to $\bar{f}_c$. This reduces the total number of equations to four. There are still five unknowns

($\{\phi_{as/cs}, \phi_{bs}, \alpha_a, \alpha_b, \alpha_c\}$), however, which means a new relationship needs to be introduced to square up the system. A new relationship of the form $\phi_{bs} = \pm 2\phi_{as}$ is introduced. The rationale behind this is that the hinge angles ϕ_a and ϕ_c actually only constitute 'half' angles, in that they span the angle from one bar to a central plane of symmetry. In the construction of a physical model, a hinge which opened to twice that value would be required to link one bar to the next. It was hypothesised that if hinge b could be set to open to twice the value of the two (equal) half-angles of hinges a and c, then perhaps a single type of hinge, designed to open only as far as a certain fixed angle, would be required to construct the entire loop. This reduced 4×4 system of polynomials has a mixed volume of only 96.

An example of some initial design parameters for a rectangular loop are given in Table 3. This time, only sixteen

Parameter	Value
Hinge a location	{1.1,0}
Hinge b location	{1.1,0.7}
Hinge c location	{0,0.7}
δ_{aX}	0.1
δ_{bY}	0.0537
δ_{cY}	0.1

Table 3. Initial parameters for rectangular 8-bar design example.

real solutions were found, but again, four of them were geometrically distinct. The four deployment paths are shown in Figure 17. The details of the one feasible design are given in Table 4. What is immediately apparent is that $\phi_{bs} \neq \pm 2\phi_{as}$.

Parameter	Value (rad)
ϕ_{as},ϕ_{cs}	1.4500
ϕ_{bs}	-3.3832
α_a	-1.0613
α_b	-1.7585
α_c	-0.8795

Table 4. Design variables for rectangular 8-bar, design # 1.

However, what is the case is that $\cos(\phi_{bs}) = \cos(2\phi_{as})$ and $\sin(\phi_{bs}) = \sin(2\phi_{as})$. This is not surprising, as the specification $\phi_{bs} = 2\phi_{as}$ has the equivalent effect on the equations of setting:

$$\cos(\phi_{bs}) = \cos^2(\phi_{as}) - \sin^2(\phi_{as})$$
$$\sin(\phi_{bs}) = 2\sin(\phi_{as})\cos(\phi_{as})$$

As it happens, no feasible solutions satisfying $\phi_{bs} = \pm 2\phi_{as}$ were found for this rectangular linkage. The folding process

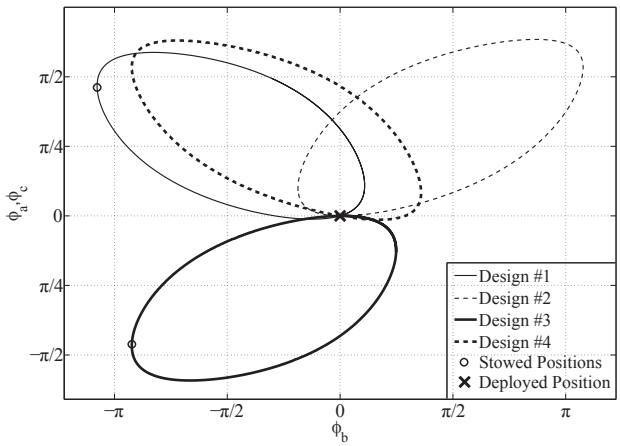

(a) The four distinct solutions

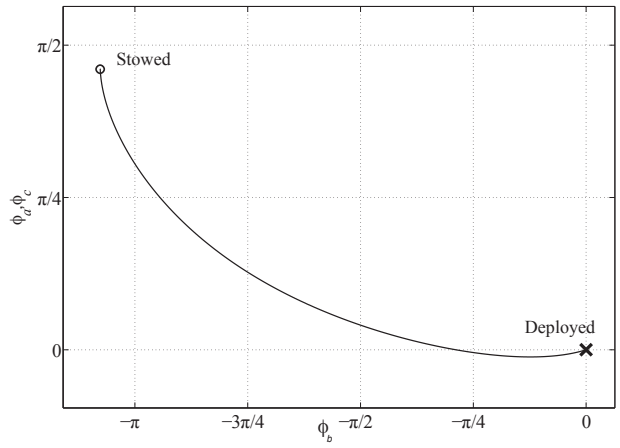

(b) Detail of only feasible solution

Fig. 17. Internal angles for rectangular 8-bar foldable ring. All simulations were started at the ring deployed positions. Only design # 1 was found to progress satisfactorily from the deployed to stowed configuration.

is shown in Figure 18. It is possible that a rectangular frame with a different aspect ratio might be deployable with $\phi_{bs} = \pm 2\phi_{as}$, but none has been found to date.

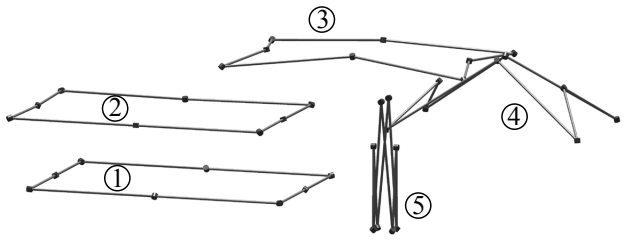

Fig. 18. Folding of rectangular 8-bar, example design # 1; clockwise from bottom left.

3.3 Note on Deployability

Rather than use a 4, 5 or 6-bar linkage, a designer might choose to use an 8-bar linkage as the basis of a deployable ring because of the greater range of deployed shapes possible, and because of the greater control which can be exercised over the way in which the frame deploys. However, some extra complications need to be considered. Many deployable frames based on 4, 5 or 6-bar linkages have only a single degree of freedom, and hence have pre-determined deployment paths which can often be easily followed simply by applying sufficient moments at one or more of the hinges [30, 31]. By their nature, 8-bar spatial linkages (arranged in a loop) will have at least two degrees of freedom. It is important that the extra benefit derived from the increased versatility in shape outweigh the increase in complexity of the deployment system. The double symmetry of the frames considered in this section means that hinge b is replicated four times around the loop, while hinges a and c are replicated twice each. If (as was the case in the examples given above), hinge angles ϕ_a and ϕ_c are set to be equal, then two distinct values of hinge angle will be present in the loop. At this stage, the best method of deploying a doubly symmetric 8-bar frame is unknown, although it is possible that a set of four identical, damped, spring-loaded hinges attached to either hinges b or a, c might suffice.

The charts displaying angles ϕ_a, ϕ_c vs. ϕ_b provide some valuable information about the deployability of a given 8-bar design. If hinge b is to be the driven hinge, then it is desirable that ϕ_b be a monotonic function of ϕ_a, ϕ_c, or if a, c is to be the driven hinge, that ϕ_a, ϕ_c be a monotonic function of ϕ_b over the deployment range. Consider design # 4 of the arbitrarily positioned vertices example, whose deployment path is shown in Figure 15. Notice that ϕ_a, ϕ_c increase/decrease monotonically, meaning that spring loaded hinges could, most likely, be used to deploy the ring without causing it to deviate from its prescribed deployment path. Next, consider design # 1 of the rectangular 8-bar example, whose deployment path is shown in Figure 17. This time ϕ_b increases/decreases monotonically with ϕ_a, ϕ_c, but the converse is not true. Hinge b presents itself as the only candidate for a driven hinge.

4 Conclusion

Polynomial continuation has been shown to be a reliable method of designing deployable spatial rings to meet certain geometric criteria. Fundamentally, the design process involves the construction of relevant compatibility equations for the basic configuration of the ring, and then solving these equations for the design variables required to allow the ring to exhibit the desired kinematic properties. Solving these compatibility equations by standard numerical techniques is unlikely to reveal a real solution, let alone the full complement of solutions. By using continuation it is possible to guarantee that every satisfactory combination of design variables has been found.

In Section 2, regular polygonal foldable rings were designed by first deriving a compatibility equation, then re-expressing that same equation several times to form a system representing a ring which passes through a prescribed series of shapes. Three different combinations of input orientation parameters were studied, and the usefulness of each combination to the design process was outlined.

In Section 3 a single compatibility equation was used in concert with a collection of constraint equations to design a (non-regular) doubly symmetric polygonal ring which was able to fold into a specified stowed shape.

If the linkage closure/compatibility equations, and the constraint equations have been posed correctly, then the use of continuation guarantees that every possible design option satisfying the imposed constraints will be found. In a second step of the design process, a designer can confidently exercise his/her judgement in deciding which of the feasible options best suits the application under consideration.

References

[1] Morgan, A., and Wampler, C., 1990. "Solving a planar four-bar design problem using continuation". *Journal of Mechanical Design,* **112**, pp. 544–550.

[2] Subbian, T., and Flugrad, D. R., 1991. "Four-bar path generation synthesis by a continuation method". *Journal of Mechanical Design,* **113**, pp. 63–69.

[3] Wampler, C. W., Morgan, A. P., and Sommese, A. J., 1992. "Complete solution of the nine-point path synthesis problem for four-bar linkages". *Journal of Mechanical Design,* **114**, pp. 153–159.

[4] Angeles, J., Alivizatos, A., and Akhras, R., 1988. "An unconstrained nonlinear least-square method of optimization of RRRR planar path generators". *Mechanism and Machine Theory,* **23**(5), pp. 343–353.

[5] Sancibrian, R., Viadero, F., García, P., and Fernández, A., 2004. "Gradient-based optimization of path synthesis problems in planar mechanisms". *Mechanism and Machine Theory,* **39**, pp. 839–856.

[6] Krishnamurty, S., and Turcic, D. A., 1992. "Optimal synthesis of mechanisms using nonlinear goal programming techniques". *Mechanism and Machine Theory,* **27**(5), pp. 599–612.

[7] Martínez-Alfaro, H., 2007. *Advances in Metaheuristics for Hard Optimization*. Springer Berlin Heidelberg, ch. Four-Bar Mechanism Synthesis for *n* Desired Path Points Using Simulated Annealing, pp. 23–37.

[8] Owen, J. C., 1991. "Algebraic solution for geometry from dimensional constraints". In ACM Symposium on Solid and Physical Modeling.

[9] Lee, H.-Y., and Liang, C.-G., 1988. "Displacement analysis of the general spatial 7-link 7R mechanism". *Mechanism and Machine Theory,* **23**(3), pp. 219–226.

[10] Chtcherba, A. D., and Kapur, D., 2004. "Constructing Sylvester-type resultant matrices using the Dixon formulation". *Journal of Symbolic Computation,* **38**, pp. 777–814.

[11] Nielsen, J., 1997. "Solving sets of nonlinear equations for the design and analysis of mechanical systems".

PhD thesis, Dept. Of Mechanical Engineering, Leland Stanford Junior University.

[12] Emiris, I. Z., 1994. "Sparse elimination and applications in kinematics". PhD thesis, University of California at Berkeley.

[13] Emiris, I. Z., and Mourrain, B., 1996. Polynomial system solving and the case of the six-atom molecule. Tech. Rep. 3075, INRIA.

[14] Morgan, A., 1987. *Solving Polynomial Systems Using Continuation for Engineering and Scientific Problems*. Prentice-Hall, inc.

[15] Wampler, C. W., Morgan, A. P., and Sommese, A. J., 1990. "Numerical continuation methods for solving polynomial systems arising in kinematics". *Journal of Mechanical Design,* **112**, pp. 59–68.

[16] Allgower, E. L., and Georg, K., 2003. *Introduction to Numerical Continuation Methods*. Society for Industrial and Applied Mathematics (SIAM).

[17] Zulehner, W., 1988. "A simple homotopy method for determining all isolated solutions to polynomial systems". *Mathematics of Computation,* **50**(181), pp. 167–177.

[18] Sommese, A. J., Verschelde, J., and Wampler, C. W., 2002. "Advances in polynomial continuation for solving problems in kinematics". In Proceedings of DETC'02, ASME Design Engineering Technical Conferences.

[19] Li, T. Y., 1999. "Solving polynomial systems by polyhedral homotopies". *Taiwanese Journal of Mathematics,* **3**(3), pp. 251–279.

[20] Li, T. Y., 2003. *Handbook of Numerical Analysis*, Vol. XI. North-Holland, ch. Numerical Solution of Polynomial Systems by Homotopy Continuation Methods, pp. 209–304.

[21] Sommese, A. J., and Wampler, C. W., 2005. *The Numerical Solution of Systems of Polynomials Arising in Engineering and Science*. World Scientific.

[22] Huber, B., and Sturmfels, B., 1995. "A polyhedral method for solving sparse polynomial systems". *Mathematics of Computing,* **64**(212), pp. 1541–1555.

[23] Viquerat, A., 2011. "Polynomial continuation in the design of deployable structures". PhD thesis, University of Cambridge.

[24] MATLAB, 2010. *version 7.10.0 (R2010a)*. The MathWorks Inc., Natick, Massachusetts.

[25] Tibert, G., 2002. "Deployable tensegrity structures for space applications". PhD thesis, Royal Institute of Technology, Department of Mechanics, Stockholm.

[26] Crawford, R. F., Hedgepeth, J. M., and Preiswerk, P. R., 1974. "Spoked wheels to deploy large surfaces in space: weight estimates for solar arrays". In Canadian Aeronautics and Space Institute and American Institute of Aeronautics and Astronautics, Joint Meeting, Toronto, Canada; United States.

[27] Crawford, R. F., Hedgepeth, J. M., and Preiswerk, P. R., 1975. Spoked wheels to deploy large surfaces in space-weight estimates for solar arrays. Tech. Rep. NASA-CR-2347; ARC-R-1004, NASA.

[28] Gao, T., and Li, T.-Y., 2003. "Mixed volume computation for semi-mixed systems". *Discrete and Computational Geometry,* **29**(2), pp. 257–277.

[29] Gan, W. W., and Pellegrino, S., 2006. "Numerical approach to the kinematic analysis of deployable structures forming a closed loop". *Journal of Mechanical Engineering Science,* **220**(C), pp. 1045–1056.

[30] Laloi, N., 1999. Analytical and experimental study of a new type of hinges. Tech. rep., Deployable Structures Laboratory, Dept. of Engineering, University of Cambridge.

[31] Pellegrino, S., Green, C., Guest, S. D., and Watt, A., 2000. SAR advanced deployable structure. Tech. rep., University of Cambridge Department of Engineering.